



1 **Intensified modulation of aerosol pollution in China by El**
2 **Niño with short duration**

3
4
5 Liangying Zeng¹, Yang Yang^{1*}, Hailong Wang², Jing Wang³, Jing Li⁴, Lili Ren¹,
6 Huimin Li¹, Yang Zhou¹, Pinya Wang¹, Hong Liao¹

7
8
9 ¹Jiangsu Key Laboratory of Atmospheric Environment Monitoring and Pollution
10 Control, Jiangsu Collaborative Innovation Center of Atmospheric Environment and
11 Equipment Technology, School of Environmental Science and Engineering, Nanjing
12 University of Information Science and Technology, Nanjing, Jiangsu, China

13 ²Atmospheric Sciences and Global Change Division, Pacific Northwest National
14 Laboratory, Richland, Washington, USA

15 ³Tianjin Key Laboratory for Oceanic Meteorology, Tianjin Institute of Meteorological
16 Science, Tianjin, China

17 ⁴Department of Atmospheric and Oceanic Sciences, School of Physics, Peking
18 University, Beijing, China

19
20
21 *Correspondence to yang.yang@nuist.edu.cn



22 **Abstract**

23 El Niño-Southern Oscillation (ENSO), a phenomenon of periodic changes in sea
24 surface temperature in the equatorial central eastern Pacific Ocean, is the strongest
25 signal of interannual variability in the climate system with a quasi-period of 2-7 years.
26 El Niño events have been shown to have important influences on meteorological
27 conditions in China. In this study, the impacts of El Niño with different durations on
28 aerosol concentrations and haze days during December-January-February (DJF) in
29 China are quantitatively examined using the state-of-the-science Energy Exascale
30 Earth System Model version 1 (E3SMv1). We find that PM_{2.5} concentrations are
31 increased by 1-2 $\mu\text{g m}^{-3}$ in the northeastern and southern China and decreased by up
32 to 2.4 $\mu\text{g m}^{-3}$ in central-eastern China during El Niño events relative to the
33 climatological means. Compared to long duration (LD) El Niño events, El Niño with
34 short duration (SD) but strong intensity causes northerly wind anomalies over
35 central-eastern China, which is favorable for aerosol dispersion over this region.
36 Moreover, the anomalous southeasterly winds weaken the wintertime prevailing
37 northwesterly in northeastern China and facilitate aerosol transport from South and
38 Southeast Asia, enhancing aerosol increase in northeastern China during SD El Niño
39 events relative to LD El Niño events. In addition, the modulation on haze days by SD
40 El Niño events is 2-3 times more than that by LD El Niño events in China. The
41 aerosol variations during El Niño events are mainly controlled by anomalous aerosol
42 accumulation/dispersion and transport due to changes in atmospheric circulation,
43 while El Niño-induced precipitation change has little effect. The occurrence frequency
44 of SD El Niño events has been increasing significantly in recent decades, especially
45 after 1940s, suggesting that El Niño with short duration have exerted increasingly
46 intense modulation on aerosol pollution in China over the past few decades.

47



48 **1. Introduction**

49 Since the beginning of the 21st century, China has experienced frequent events of
50 heavy haze pollution (Yang et al., 2018). The excessive aerosol concentrations during
51 the heavy haze events can cause a large decrease in atmospheric visibility (Han et al.,
52 2013) and pose significant public health hazards, such as a dramatic increase in
53 cardiovascular and respiratory diseases and associated mortality rates (Liu et al.,
54 2019). PM_{2.5} (particulate matter less than 2.5 μm in diameter) has been reported to be
55 the fifth leading risk factor for mortality, inducing 7.6% of total deaths globally in
56 2015 (Cohen et al., 2017). In order to alleviate air pollution, China has been
57 continuously taking clean air actions in the recent years to battle for the blue sky. If all
58 goes as planned, by 2035, the quality of atmospheric environment will be
59 fundamentally improved and the goal of a beautiful China will be basically achieved.
60 However, this goal requires a comprehensive and better scientific understanding of all
61 factors that can affect aerosol concentrations and haze pollution in China.

62 Undoubtedly, the rise of anthropogenic emissions is the fundamental reason for
63 the increase in aerosol concentration and haze pollution events (Huang et al., 2014),
64 but the unfavorable meteorological condition, as one of the most important external
65 factors, has been reported to have substantial influences on haze formation (Yang et
66 al., 2016a; Wang et al., 2019, 2020a). With increasing greenhouse gases in the future
67 (2050-2099), severe winter haze events in Beijing would become 50% more frequent
68 and 80% longer in duration, compared to the historical period (1950-1999), due to an
69 accelerated warming of the lower atmosphere and weakening of the East Asian winter
70 monsoon (Cai et al., 2017). In addition, external forcings, such as Pacific Decadal
71 Oscillation (Zhao et al., 2016) and Arctic sea ice (Wang et al., 2015; Zou et al., 2020),
72 all have important impacts on aerosol concentrations and haze pollution in China. El
73 Niño-Southern Oscillation (ENSO), as another prominent climate phenomenon
74 caused by the coupled atmosphere-ocean interactions in the tropical Pacific Ocean
75 (Trenberth, 2019), is a significant signal of interannual climate change on a global
76 scale. It triggers atmospheric circulation and precipitation anomalies globally (Yang et
77 al., 2016b, 2016c) and certainly have an important impact on haze events and aerosol
78 concentrations in China by modulating the East Asian winter monsoon system (Sakai
79 and Kawamura, 2009; Wang et al., 2000; Zhang et al., 2017).

80 The ENSO cycle is composed of warm-phase (i.e., El Niño) and cool-phase (i.e.,



81 La Niña) of sea surface temperatures (SSTs) over the tropical eastern Pacific Ocean,
82 which further cause precipitation, atmospheric circulation and temperature anomalies
83 in much of the tropics and subtropics. Such changes also affect the spatiotemporal
84 distribution of aerosols in China (Feng et al., 2017, 2020; Sun et al., 2018; Yang et al.,
85 2014; Zhao et al., 2018; Zhu et al., 2012; Wang et al., 2020b). During a strong El
86 Niño event in 2015/2016, PM_{2.5} concentrations in winter were observed to increase by
87 20-100 µg/m³ in eastern China compared to that in 2014, which was attributed to the
88 weakened wind speed in the North China Plain during the El Niño event (Chang et al.,
89 2016; Wang et al., 2020a). PM_{2.5} concentrations in southern China were also
90 decreased by about 20 µg/m³ during the 2015/2016 El Niño event, which was
91 attributed to an enhanced precipitation and aerosol wet scavenging over this region.
92 Based on haze day counting mainly using atmospheric visibility, many studies found
93 that El Niño events could induce more (fewer) winter haze days in northern (southern)
94 China (Gao and Li, 2015; Li et al., 2017). In addition to surface observations, several
95 studies have also analyzed the relationship between ENSO events and aerosol loading
96 based on aerosol optical depth (AOD) data from satellite retrievals. Jeoung et al.
97 (2014) analyzed the combined AOD data of MODIS (Moderate Resolution Imaging
98 Spectroradiometer), MISR (Multi-angle Imaging SpectroRadiometer) and AERONET
99 (Aerosol Robotic Network) and found that during the warm phase of ENSO, the
100 fine-mode AOD increased in eastern coastal areas but decreased in some inland areas
101 of China. Sun et al. (2018) studied the influence of ENSO events on the interannual
102 variation of wintertime aerosol in China using AOD data (1980-2016) from
103 MERRA-2 reanalysis and found that AOD in the North China Plain increased
104 significantly during El Niño events, with a 15% increment in the
105 Beijing-Tianjin-Hebei region compared to the long-term average. They also pointed
106 out that AOD increased in eastern and southern China and decreased in southwestern
107 China during El Niño events.

108 Although observational data showed that aerosols in China were largely
109 perturbed during El Niño events, the individual impacts of atmospheric circulation
110 and precipitation anomalies associated with El Niño could not be simply extracted out
111 with observations alone. Numerical simulations have been used to isolate the
112 individual impacts of El Niño on aerosols in China through a superposed SST
113 perturbation method and explore the underlying mechanisms (Yu et al., 2019; Zhao et
114 al., 2018). Based on an aerosol-climate coupling model, Zhao et al. (2018) suggested



115 that El Niño increased the seasonal mean aerosol concentration in southern China in
116 winter, which is mainly due to the increased aerosol transport from South and
117 Southeast Asia. Using the same model, Yu et al. (2019) showed that, relative to the
118 climatological mean, wintertime surface aerosol concentrations in northeastern and
119 southeastern China (central and southwestern China) increased (decreased) during El
120 Niño events, which was mainly attributed to anomalies in near-surface winds and the
121 resulting aerosol mass flux divergences. Sun et al. (2018) used the aerosol-climate
122 model CAM5 to simulate the impact of ENSO events on the interannual variability of
123 AOD in China and found that El Niño events led to an increase in AOD in central and
124 eastern China. They suggested that the change in AOD was mainly dominated by the
125 change in meridional winds.

126 Some studies focused on the effects of different spatial types (e.g., East Pacific
127 and Central Pacific El Niño, Kao and Yu (2009)) and intensities of El Niño events on
128 aerosol concentrations in China (e.g., Yu et al., 2019). Yu et al. (2019) found that, due
129 to the difference in atmospheric circulation between two types of El Niño, Central
130 Pacific El Niño events resulted in a larger increase in aerosol burden in southern
131 China than East Pacific El Niño events. They also indicated that a moderate El Niño
132 event led to an increase in seasonal mean near-surface aerosol concentrations
133 throughout eastern China in winter, while a strong or weak El Niño event brought
134 about a significant decrease in aerosol concentrations in northern China.

135 Apart from the spatial types, El Niño can also be categorized as short duration
136 (SD) and long duration (LD) according to the length of their decay period (Boo et al.,
137 2004; Chen et al., 2012; Guo and Tan, 2018). These two temporal types of El Niño
138 events have been confirmed to have different impacts on the SSTs, vertical wind shear,
139 relative humidity and precipitation in South China Sea and Philippine Sea (Guo and
140 Tan, 2018; Wu et al., 2019). The El Niño events with different durations are likely to
141 have different impacts on the aerosol distribution in China. However, few studies
142 explore the different impacts of SD and LD El Niño events on aerosol concentrations
143 and haze days in China, as well as the associated mechanisms, which are essential for
144 air pollution control in the near future.

145 In this study, the effects of SD and LD El Niño events on wintertime aerosols in
146 China are investigated by using the state-of-the-science Energy Exascale Earth
147 System Model (E3SM). The data, model, and analysis methods used in this research
148 are presented in Section 2. The influences of different durations of El Niño events on



149 aerosols over China and the mechanisms involved are analyzed in Section 3.
150 Summary of the main results and discussion of the implications for future research are
151 provided in Section 4.

152 **2. Data and Methods**

153 **2.1 Data**

154 We use the following datasets in this study.

155 (1) The merged Hadley-NOAA/OI SST and sea ice concentration (SIC) datasets
156 from 1870 to 2017 with a horizontal resolution of $1^\circ \times 1^\circ$ (Hurrell et al., 2008)
157 are used to obtain the climatological mean SST and SIC pattern and the
158 anomalies of SST during SD and LD El Niño events.

159 (2) Monthly mean emissions of aerosols and their precursors in 2014 from the
160 CMIP6 (Coupled Model Intercomparison Project Phase 6) (Hoesly et al.,
161 2018; van Marle et al., 2017) with emissions in China replaced by MEIC
162 (multi-resolution emission inventory for China) emission inventory are used
163 as input datasets in model simulations.

164 (3) Hourly observations of $PM_{2.5}$ concentrations at 1657 stations over China
165 from December 2014 to February 2015 derived from the China National
166 Environmental Monitoring Centre (CNEMC) (<http://www.cnemc.cn>) are
167 applied to evaluate the model performance.

168 **2.2 SD and LD El Niño events**

169 Here we first describe how the LD and SD El Niño events are defined. The year
170 in which El Niño developed is denoted by year⁰ and the months of that year is denoted
171 by Jan⁰, Feb⁰, ..., and Dec⁰, while the following year and months are year¹ and Jan¹,
172 Feb¹, ..., and Dec¹, respectively. Each El Niño event is firstly identified when a
173 3-month running mean Niño 3.4 index, defined as the regional mean linear detrended
174 SST anomaly from the monthly mean climatology over the Niño3.4 region
175 (170°W - 120°W , 5°S - 5°N), is greater than 0.75°C in any month from Oct⁰ to Feb¹ of
176 the developing phase. If the Niño 3.4 index is higher than 0.5°C in any month from
177 Oct¹ to Feb² of the decaying phase, the El Niño event is an LD El Niño event;
178 otherwise, it is an SD El Niño event (Wu et al., 2019).

179 Figure 1 shows the time series of the Niño3.4 indices calculated based on the
180 Hadley-NOAA/OI data for the period 1870-2017. According to the definition above,
181 totally 30 El Niño events are identified in this time period, with 22 SD El Niño events



182 (1877/1878, 1885/1886, 1888/1889, 1896/1897, 1902/1903, 1911/1912, 1923/1924,
183 1925/1926, 1930/1931, 1951/1952, 1957/1958, 1963/1964, 1965/1966, 1972/1973,
184 1982/1983, 1991/1992, 1994/1995, 1997/1998, 2002/2003, 2006/2007, 2009/2010,
185 2015/2016 as developing phase) and 8 LD El Niño events (1899/1900, 1904/1905,
186 1913/1914, 1918/1919, 1939/1940, 1968/1969, 1976/1977, 1986/1987 as developing
187 phase). The temporal evolution of the Niño3.4 indices during the developing and
188 decaying phases of SD and LD El Niño events are shown in Figure 2. During the
189 developing phase from Jul⁰ to Feb¹, due to the fast accumulation of ocean heat content
190 and rapid adjustments of the surrounding seas to the tropical Pacific Ocean warming
191 (Wu et al., 2019), the Niño3.4 indices are higher in SD El Niño events, but the SST
192 decreases rapidly in the decaying phase, compared to those in LD events.

193 **2.3 Model description and experimental design**

194 To quantify the influence of El Niño with various durations on aerosols in China,
195 the U.S. Department of Energy (DOE) E3SM version 1 (E3SMv1) is utilized in this
196 study, which includes atmosphere, land, ocean, sea ice and river components (Golaz et
197 al., 2019). It was branched from the CESM1 (Community Earth System Model) but
198 has been updated substantially since. The E3SM Atmosphere Model version 1
199 (EAMv1) is a descendant of the well-known CAM5.3 (Community Atmosphere
200 Model version 5.3) (Rasch et al., 2019). It includes considerable upgrades to aerosols,
201 turbulence, chemistry and cloud related processes. EAMv1 provides various options
202 of spatial resolution. In this study, the horizontal spatial resolution of approximately
203 1° and 30 vertical layers from the surface to 3.6 hPa are used in the model
204 configuration. The model simulates aerosols including sulfate, black carbon (BC),
205 primary organic aerosol (POA), secondary organic aerosols (SOA), sea salt, and
206 mineral dust in the four-mode Modal Aerosol Module (MAM4) (Wang et al., 2020).

207 The following numerical experiments are conducted in this study. A “CLIM”
208 experiment is driven by climatological average of monthly SST and SIC over
209 1870-2017 and integrated for 20 years. Two sets of sensitivity experiments, “SD” and
210 “LD”, are respectively driven by the monthly SST representing composite SD and LD
211 El Niño events. The monthly SSTs representing SD (LD) El Niño events are produced
212 through superposing the average of monthly SSTs from Jul⁰ to Jun¹ of the 22 SD (8
213 LD) El Niño events selected in Sec. 2.2 on top of the climatological monthly SST
214 over 60°S-60°N. Each set of sensitivity experiment has 3 ensemble members with
215 different initial conditions branched from different years of the CLIM experiment.



216 Each member of the sensitivity experiments is run for 8 years with first 3 years used
217 for spin-up and the last 5 years used for analysis. The differences in the monthly and
218 daily mean model fields between SD, LD and CLIM are used to analyze the effects of
219 duration of El Niño events on aerosols. To understand the potential mechanism of El
220 Niño impacts on aerosol pollution in China, two additional experiments are also
221 conducted. The “SD_emis” experiment is the same as the first ensemble member of
222 SD experiment, except that the emissions of aerosols and precursor gases from South
223 and Southeast Asia are turned off. The “CLIM_emis” experiment is same as the
224 “SD_emis” experiment but driven by climatological average of monthly SST and SIC
225 over 1870-2017. All other external forcings, including insolation, greenhouse gas
226 concentrations, and emissions of aerosol and precursor are kept at present-day
227 conditions (year 2014), In brief, the experiments performed are as follows.

- 228 1. CLIM: control simulation driven by climatological SST.
- 229 2. SD: sensitivity simulation to quantify the impacts of El Niño events with
230 short duration on aerosols in China. Same as CLIM except for the imposed
231 SST pattern of short duration El Niño.
- 232 3. LD: sensitivity simulation to quantify the impacts of El Niño events with
233 long duration on aerosols in China. Same as CLIM except for the imposed
234 SST pattern of long duration El Niño.
- 235 4. SD_emis: sensitivity simulation to quantify the role of regional transport of
236 aerosols from South and Southeast Asia on aerosols in China during El Niño
237 events with short duration. Same as SD except that the emissions of aerosols
238 and precursor gases from South and Southeast Asia are turned off.
- 239 5. CLIM_emis: sensitivity simulation to serve as the baseline for SD_emis.
240 Same as SD_emis except for the use of climatological SST.

241 **2.4 Model evaluation**

242 To evaluate the model performance in simulating aerosol concentration and
243 distribution in China, the simulated December-January-February (DJF) mean surface
244 PM_{2.5} (sum of sulfate, BC, POA and SOA in model simulation) concentrations from
245 the CLIM experiment is compared with the observed PM_{2.5} concentrations in Fig. 4.
246 The model well reproduced the spatial distribution of wintertime aerosols in China,
247 with high aerosol concentrations in eastern China (e.g., North China Plain, Fenwei
248 Plain and Yangtze River Delta) and southwestern China (e.g., Sichuan Basin) and low
249 aerosol levels in western China. The spatial correlation coefficient (R) between the



250 E3SMv1 EAMv1 simulation and observations for near-surface PM_{2.5} concentrations is
251 +0.43. However, the model underestimates the PM_{2.5} concentrations in China, with a
252 normalized mean deviation (NMB) of -65.74% compared to the observed values,
253 which was also reported in many studies using the CESM1 model (e.g., Yang et al.,
254 2017a, b). The discrepancy could be due to many factors, including the lack of nitrate
255 and ammonium aerosols in the model, strong wet scavenging simulated at the mid-
256 and high latitudes, and less transformation from gas to particles. In addition, we focus
257 on anthropogenic aerosols. If natural dust is considered in the modeled PM_{2.5}
258 calculation, the NMB will drop to -6.38%. Nevertheless, the aerosol concentrations in
259 EAMv1 simulations are closer to the observations than previous ENSO-aerosol
260 studies (e.g., Yu et al., 2019; Zhao et al., 2018) and the composite differences are
261 analyzed in this study rather than the climatological mean concentration. We don't
262 expect the systematic low biases in PM_{2.5} concentrations affect our study on the
263 impact of El Niño events. However, we should note that the aerosol changes in China
264 during SD/LD El Niño events in the real world could be larger than the simulated
265 values here.

266

267 **3. Results**

268 **3.1 Impacts of SD and LD El Niño events on aerosol concentrations**

269 Figures 5 and 6 show the absolute and relative impacts, respectively, of the two
270 types of El Niño events with different durations on the simulated DJF mean
271 near-surface concentrations and column burdens of PM_{2.5} in China. The effects of the
272 SD and LD El Niño events on near-surface aerosol concentrations over China are
273 similar in the spatial pattern distribution, with increases in the northeastern and
274 southern China by about 1-2 μg m⁻³ (5-15% compared to the climatological mean)
275 and decreases in central-eastern China during El Niño events relative to the
276 climatological averages. This spatial pattern of aerosol changes is in accordance with
277 previous modeling studies (Feng et al., 2016; Yu et al., 2019; Zhao et al., 2018).
278 However, the modeling results are not exactly the same as the observed PM_{2.5} changes,
279 which show increases in PM_{2.5} over northeastern China and the North China Plain and
280 slightly decreases in southern China during the 2015/2016 El Niño event (Chang et al.,
281 2016). The discrepancy between the model simulations and observations can be
282 attributed to the following reasons. First of all, instead of the El Niño impacts,



283 observed aerosols can be affected by other factors including East Asian winter
284 monsoon (Yang et al., 2016a), Arctic Oscillation (Zhang et al., 2019) and Pacific
285 Decadal Oscillation (Zhao et al., 2017), whereas the modeled changes are purely
286 caused by the El Niño impacts through the imposed SST perturbation. Secondly, the
287 time coverage of near-surface PM_{2.5} observations is limited in China and only one
288 extreme El Niño event (2015/2016) was analyzed in previous El Niño-PM_{2.5} studies
289 (e.g., Chang et al., 2016), which is not fully representative of the impact of general El
290 Niño events.

291 Although the spatial patterns of the SD and LD El Niño influences on the DJF
292 PM_{2.5} concentrations in China resemble each other, the magnitudes of the influences
293 are different. Central-eastern China experiences more reductions in near-surface PM_{2.5}
294 concentrations during SD El Niño, with the concentration decreases of more than 2.4
295 $\mu\text{g m}^{-3}$ (15% relative to the climatological mean), which is much larger than the 0.6
296 $\mu\text{g m}^{-3}$ (5%) during LD El Niño. In southern China, the spatial coverage of the
297 increase in PM_{2.5} concentration shrinks more during SD than LD El Niño events
298 relative to the CLIM, but the intensities of the anomalies triggered by the two
299 temporal types of El Niño events are similar. Moreover, SD El Niño induces a larger
300 increase in PM_{2.5} concentrations in northeastern China by 1.2 $\mu\text{g m}^{-3}$ (10%) than that
301 of 0.6 $\mu\text{g m}^{-3}$ (5%) during LD El Niño events.

302 The PM_{2.5} burden and near-surface concentration anomalies triggered by the El
303 Niño events with short and long durations are basically the same in spatial distribution
304 but with different magnitudes (Fig. 5). For example, the reduction in aerosol burden is
305 much larger in central-eastern China during the SD El Niño events than during the LD
306 El Niño events, with maximum negative anomalies, respectively, reaching -1.6 and
307 -0.6 mg m^{-2} . Overall, SD El Niño events yield stronger impacts on aerosol pollution in
308 China than LD El Niño events, especially in central-eastern China with negative
309 pollution anomalies.

310 **3.2 Mechanisms of SD and LD El Niño impacts on aerosols**

311 Since aerosols and their precursor gas emissions are prescribed at the same rates
312 in the control (CLIM) and SD/LD sensitivity simulations, changes in meteorological
313 factors such as circulation and precipitation play dominant roles in altering aerosol
314 concentrations by influencing the regional transport and wet removal of aerosols
315 (Yang et al., 2016a). Previous studies also suggested that aerosol variations during
316 ENSO events were controlled by ENSO-related circulation and precipitation changes



317 (Yu et al., 2019; Zhao et al., 2018). Here, we examine the atmospheric circulation and
318 precipitation anomalies and the associated aerosol processes during the SD and LD El
319 Niño to explore the mechanisms of the two types of El Niño effects on aerosols in
320 China.

321 Both the SD and LD El Niño events trigger negative anomalies in sea level
322 pressure (SLP) over the eastern China and East China Sea and positive anomalies
323 over the Philippine Sea and Sea of Okhotsk (not shown), leading to anomalous
324 cyclonic and anticyclonic circulations over these regions, respectively (Figs. 7a and
325 7b). At 850 hPa, the anomalous cyclonic circulation over the East China Sea causes
326 anomalous northerly winds over central-eastern China, enhancing the prevailing
327 northwesterly winds in winter. The enhanced winds favor the aerosol dispersion,
328 which explains the decrease in $PM_{2.5}$ concentrations over central-eastern China during
329 El Niño events relative to the climatological mean. In addition, at 500 hPa, most areas
330 over China have an anomalous low pressure (Figs. 7d and 7e), which increases the
331 atmospheric instability and strengthens the aerosol vertical mixing and dispersion
332 over central-eastern China. Over southern China, the aerosol variations are
333 significantly affected by the regional transport of particles from South and Southeast
334 Asia. During El Niño events, anomalous southwesterly winds at the northwest edge of
335 the anomalous anticyclone over the Philippine Sea bring aerosols from South and
336 Southeast Asia to southern China, contributing to the aerosol increases in southern
337 China relative to the climatological mean (Figs. 7a and 7b). In the northeastern China,
338 anomalous southeasterly winds associated with the anomalous anticyclonic circulation
339 over Sea of Okhotsk weaken the wintertime prevailing northwesterly winds, giving
340 rise to the aerosol increases in the northeastern China during El Niño events. In
341 addition, the anomalous anticyclone brings aerosols from South and Southeast Asia to
342 northeastern China that will be discussed next, contributing to the aerosol pollution in
343 northeastern China during El Niño events.

344 Compared to LD El Niño events, the negative anomaly of SLP over the East
345 China Sea during the SD El Niño events is stronger and extends deeply into the
346 central-eastern China, resulting in anomalous northerly winds over central-eastern
347 China and southeasterly winds over northeastern China in the lower atmosphere (Fig.
348 7c). The wind anomalies intensify the aerosol dispersion in central-eastern and
349 accumulation in northeastern China, leading to a stronger effect of El Niño with short
350 duration on the aerosol variation in China. Furthermore, the anomalous northerly



351 winds in both lower atmosphere and 500 hPa over southern China (Figs. 7c and 7f)
352 are uncondusive to the regional transport of aerosols from South and Southeast Asia
353 to central-eastern China.

354 In addition to the regional transport prompted by anomalous atmospheric
355 circulations, El Niño can influence aerosol wet removal through perturbing
356 precipitation. As described in Figs. 8a and 8b, the spatial patterns of winter
357 precipitation anomalies in China during SD and LD El Niño events are similar, with
358 positive anomalies located along the southeastern coastal areas due to the additional
359 moisture transport by anomalous southwesterly winds over the South China Sea.
360 However, the two types of El Niño events differ in the magnitude of precipitation
361 anomalies. In central-eastern China, precipitation decreases during SD El Niño events,
362 compared to LD El Niño events, whereas precipitation increases over eastern coastal
363 areas and northeastern China (Fig. 8c). This is linked to the anomalous cyclonic
364 circulation over central-eastern China (Fig. 7c), which hinders moisture from South
365 China Sea to central-eastern China but brings in moisture from Sea of Japan to
366 northeastern China. Over Pearl River Delta, precipitation decreases during SD El
367 Niño events but increases during LD El Niño events, which is also associated with the
368 anomalous northerly winds and corresponding impact on moisture transport over this
369 region. In general, aerosol wet deposition decreases in central-eastern China and
370 increases over southern and northeastern China during El Niño events (Figs. 8d and
371 8e). With short duration but strong intensity, El Niño events have larger impacts on
372 aerosol wet removal than those with long duration (Fig. 8f). However, the wet
373 removal shows a positive relationship with the aerosol concentration, which should be
374 a negative relationship in theory if other conditions remain unchanged. Therefore, the
375 differences in aerosols triggered by El Niño events with different durations are
376 primarily due to the impact of changes in atmospheric circulation on the accumulation
377 and transport of aerosols rather than the impact of precipitation on aerosol removal.

378 Both the accumulation/dispersion of local aerosols within China and regional
379 transport of aerosols from South and Southeast Asia can contribute to the aerosol
380 changes in China during El Niño events. With emissions of aerosols and precursor
381 gases in South and Southeast Asia turned off, the decrease pattern of PM_{2.5} over
382 central-eastern China does not change (Fig. 9), suggesting that
383 accumulation/dispersion of local aerosols dominates the aerosol change over this
384 region during El Niño events. Over southern China, the increase of PM_{2.5} burden is



385 weakened when the South and Southeast Asian emissions are turned off, indicating
386 that regional transport of aerosols from South and Southeast Asia have a large
387 contribution to the aerosol variation over this region. It is interesting that, without
388 emissions from South and Southeast Asia, both near-surface concentration and
389 column burden of $PM_{2.5}$ in northeastern China decrease during El Niño events relative
390 to the climatological mean, but the change reverses to increase when the South and
391 Southeast Asian emissions are considered. It indicates that the aerosol enhancements
392 in northeastern China during the El Niño events are most likely influenced by aerosol
393 transport from South and Southeast Asia due to anomalous southeasterly winds at the
394 eastern edge of the anomalous cyclonic circulation in eastern China (Fig.7c), which
395 warrants further analysis using a source-receptor model such as CAM5-EAST (Ren et
396 al., 2020; Yang et al., 2020).

397 **3.3 Quantitative impacts on regional $PM_{2.5}$ concentrations and haze** 398 **days**

399 Table 1 summarizes the simulated regional mean $PM_{2.5}$ concentrations and
400 number of haze days in DJF over the sub-regions in China (Fig. 10), including the
401 North China Plain (NCP, 35–41°N, 114–120°E), Sichuan Basin (SCB, 28–33°N,
402 103–108°E), Yangtze River Delta (YRD, 29–34°N, 118–121.5°E), Pearl River Delta
403 (PRD, 21.5–25°N, 111–116°E), Northeast Plain (NEP, 41–48°N, 120–130°E), the
404 Yunnan-Guizhou Plateau (YGP, 23–27°N, 100–110°E), and the Fenwei Plain (FWP,
405 33–35°N, 106–112°E and 35–38°N, 110–114°E) from CLIM, SD and LD simulations.
406 Haze days are defined as days with daily near-surface $PM_{2.5}$ concentrations above the
407 90th percentile of the CLIM $PM_{2.5}$ concentrations in each sub-region of China.

408 During El Niño events, DJF mean near-surface $PM_{2.5}$ concentrations decrease
409 over NCP, SCB, YGP, and FWP regions and increase over PRD and NEP in both SD
410 and LD, compared to CLIM. Although the $PM_{2.5}$ concentrations show an increase in
411 SD and a decrease in LD over YRD region, the changes are statistically insignificant
412 in this region (Fig. 5). SD El Niño events have a stronger modulation on aerosols in
413 China than LD El Niño events. Over the regions with concentration decreases (NCP,
414 SCB, YGP, and FWP), regional mean near-surface $PM_{2.5}$ concentration in LD is lower
415 than CLIM by $0.24 \mu\text{g m}^{-3}$, while the reduction reaches $1.22 \mu\text{g m}^{-3}$ in SD, about 5
416 times as that of LD. Over the regions with concentration increases (PRD and NEP),
417 the $PM_{2.5}$ increase in SD relative to CLIM is $0.74 \mu\text{g m}^{-3}$, which is also higher than
418 the $0.56 \mu\text{g m}^{-3}$ in LD.



419 Similar to the $PM_{2.5}$ concentration, the modulation of SD El Niño events on haze
420 days are 2-3 times as high as that of LD El Niño events. During LD El Niño events,
421 the number of haze days in DJF at NCP, SCB and FWP is reduced by 1.14, 0.73 and
422 1.53 days, respectively, compared to the climatological mean, while the decrease in
423 haze days during SD El Niño events is more substantial (1.87, 2.13 and 2.87 days).
424 The probability density distributions of $PM_{2.5}$ concentrations over NCP, SCB and
425 FWP in SD and LD also shift to the left, relative to CLIM (Fig. 11). Consistent with
426 the stronger modulation of SD El Niño events discussed above, the shift in SD is more
427 than that in the LD simulation. In addition, YRD, PRD and NEP regions all have
428 increases in haze days in DJF during SD and LD, relative to CLIM. Similarly, during
429 SD and LD El Niño events, the probability density distributions of high values of
430 $PM_{2.5}$ concentrations over YRD, PRD and NEP slightly shift to the right relative to
431 CLIM. The number of haze days in DJF over YGP decreases during SD El Niño
432 events by 1.4 days, but there is a slight increase of 0.4 days during LD El Niño events,
433 likely due to the opposite aerosol changes in the eastern and western parts of YGP
434 region (Fig. 5). There are more (fewer) haze days in both SD and LD than in CLIM
435 over YRD, PRD and NEP (NCP, SCB and FWP), which is inconsistent with the
436 simulated greater (less) precipitation over these regions caused by El Niño events. It
437 further indicates that anomalies in precipitation are not the most dominant factor
438 modulating winter haze days in China during El Niño events, but rather the
439 anomalous aerosol accumulation/dispersion and transport due to anomalous
440 atmospheric circulation.

441 **3.4 Historical increase in SD El Niño events**

442 Many studies have suggested an increase in the variability of El Niño events
443 under greenhouse warming (Cai et al., 2018; Grothe et al., 2020). However, few
444 studies have shown the historical changes in El Niño with different durations, which
445 would further impact aerosol concentrations and haze days in China.

446 Here we show the occurrence of SD and LD El Niño events since the
447 preindustrial era in Fig. 12. The number of SD El Niño events fluctuated but has
448 increased significantly during the past few decades, especially after 1940s. The
449 occurrence of SD El Niño increased from one event per fifteen years during
450 1941–1955 to four events per fifteen years during 2001–2015, with the increase at
451 confidence level of 92%, while LD El Niño events did not present a significant trend
452 in the historical period. Wu et al. (2019) found that the duration of El Niño is mainly



453 influenced by the timing of onset, associated with the early onset of delayed negative
454 oceanic feedback as well as the fast adjustments of the tropical Indian and Atlantic
455 Oceans to the tropical Pacific Ocean warming. It is conjectured that the onset timing
456 of El Niño events gets earlier under greenhouse forcing, but the detailed analysis is
457 out of the scope of this study. Nevertheless, because the frequency of the El Niño
458 events with short duration increased significantly, the modulation by El Niño events
459 on wintertime aerosols in China has intensified in the past few decades.

460

461 **4. Conclusion and discussions**

462 As a prominent climate phenomenon, El Niño triggers atmospheric circulation
463 and precipitation anomalies on a global scale, thus having important effects on haze
464 days and aerosol pollution in China. In this study, the impacts of different temporal
465 types of El Niño events with short and long duration on aerosols in China are
466 simulated using the state-of-the-science E3SM model.

467 For both SD and LD El Niño events, their changes to the DJF mean $PM_{2.5}$
468 concentrations have similar spatial distributions over China, relative to the
469 climatological mean. The anomalous anticyclonic circulation over the Sea of Okhotsk
470 weakens the prevailing northwesterly winds in DJF in northeastern China and
471 enhances the accumulation of locally emitted aerosols, along with the anomalous
472 southeasterly winds at the eastern edge of the anomalous cyclonic circulation in
473 eastern China that intensifies the aerosol transport from South and Southeast Asia to
474 northeastern China. The near-surface $PM_{2.5}$ concentration in northeastern China
475 increases by $1-2 \mu\text{g m}^{-3}$ during El Niño events relative to the climatological conditions.
476 In southern China, the anomalous anticyclonic circulation over the Philippine Sea
477 facilitates the transport of aerosols from South and Southeast Asia to southern China
478 and thus the near-surface $PM_{2.5}$ concentrations in southern China increase by $1-2 \mu\text{g m}^{-3}$.
479 The decrease in near-surface $PM_{2.5}$ concentrations in central-eastern China is
480 mainly controlled by the enhanced northerly winds from the anomalous cyclonic
481 circulation over eastern China and the East China Sea, leading to the dispersion of
482 local aerosols, while precipitation change has little effect on aerosols here. Compared
483 to LD El Niño events, due to the anomalous cyclonic circulation over eastern China,
484 SD El Niño events exhibit a stronger reduction ($1-2 \mu\text{g m}^{-3}$) in near-surface $PM_{2.5}$
485 concentrations over central-eastern China and a larger increase ($0.6 \mu\text{g m}^{-3}$) in



486 northeastern China. Overall, El Niño with short duration has a stronger modulation on
487 wintertime aerosols in China than El Niño with long duration.

488 Compared with CLIM, mean near-surface PM_{2.5} concentrations in DJF decrease
489 over NCP, SCB, YKP and FWP regions and increase over PRD and NEP in both SD
490 and LD, but the decrease over these regions in SD El Niño events reaches 1.22 µg m⁻³,
491 about 5 times as large as that of LD. Similarly, both SD and LD El Niño events induce
492 less (more) haze days in DJF than CLIM over NCP, SCB and FWP (YRD, PRD and
493 NEP). However, the decreases in haze days in DJF at NCP, SCB and FWP during SD
494 El Niño events are 2-3 times more than that during LD El Niño events.

495 We also found that the occurrence frequency of SD El Niño events increased
496 from one event per fifteen years during 1941–1955 to four events per fifteen years
497 during 2001–2015, whereas LD El Niño events did not exhibit a significant trend in
498 the historical period. In particular, seven SD El Niño events have occurred since the
499 1990s, but no LD El Niño event occurred. Compared to LD El Niño events, SD El
500 Niño events have a greater impact on wintertime aerosols over China. Therefore, the
501 impact of El Niño events on wintertime aerosols in China has intensified in the past
502 few decades due to their short durations.

503 Our results of the important effect of SD El Niño events and its recent
504 intensification are of great significance for the understanding of El Niño on China's
505 haze pollution, alleviating air pollution, and coping with climate change. The
506 simulated spatial patterns of aerosol changes during El Niño events resemble those in
507 previous studies (Feng et al., 2016; Yu et al., 2019; Zhao et al., 2018). However, there
508 are still some inadequacies remaining to be improved. Natural aerosols including dust
509 and sea salt were not considered in this study. The EAMv1 model largely
510 underestimated PM_{2.5} concentration in China related to the lack of nitrate and
511 ammonium aerosols and other model biases. We also found that, during El Niño
512 events, more aerosols from South and Southeast Asia can be transported to
513 northeastern China, leading to an increase in aerosol concentrations over there. Thus,
514 more in-depth analysis is needed in future studies. In addition, during the cooling
515 phase of ENSO, La Niña events may also have various durations and can have
516 different impacts on air pollutions in China, which merits further investigation.

517
518



519 ***Data availability***

520 The E3SMv1 model is available at <https://e3sm.org/> (last access: 1 February 2021).
521 Our results can be made available upon request. Hourly observations of PM_{2.5}
522 concentrations over China can be derived from the China National Environmental
523 Monitoring Centre (<http://www.cnemc.cn>, last access: 1 February 2021)

524

525 ***Author contributions***

526 YY designed the research. LZ performed the model simulations and analyzed the data.
527 All the authors discussed the results and wrote the paper.

528

529 ***Competing interests***

530 The authors declare that they have no conflict of interest.

531

532 ***Acknowledgments***

533 This study was supported by the National Natural Science Foundation of China (grant
534 41975159) and the National Key Research and Development Program of China (grant
535 2020YFA0607803 and 2019YFA0606800). HW acknowledges the support by the U.S.
536 Department of Energy (DOE), Office of Science, Office of Biological and
537 Environmental Research (BER), as part of the Earth and Environmental System
538 Modeling program. The Pacific Northwest National Laboratory (PNNL) is operated
539 for DOE by the Battelle Memorial Institute under contract DE-AC05-76RLO1830.

540

541

542

543



544 References

545

546 Boo, K.-O., Lim, G.-H., and Kim, K.-Y.: On the low-level circulation over the western
547 north Pacific in relation with the duration of El Niño, *Geophys. Res. Lett.*, 31,
548 L10202, <https://doi.org/10.1029/2004GL019418>, 2004.

549 Cai, W., Li, K., Liao, H., Wang, H., and Wu, L.: Weather conditions conducive to
550 Beijing severe haze more frequent under climate change, *Nature Clim. Change*, 7,
551 257-262, <https://doi.org/10.1038/nclimate3249>, 2017.

552 Cai, W., Wang, G., Dewitte, B., Wu, L., Santoso, A., Takahashi, K., Yang, Y., Carréric,
553 A., and McPhaden, M. J.: Increased variability of eastern Pacific El Niño under
554 greenhouse warming, *Nature*, 564, 201-206,
555 <https://doi.org/10.1038/s41586-018-0776-9>, 2018.

556 Chang, L., Xu, J., Tie, X., and Wu, J.: Impact of the 2015 El Niño event on winter air
557 quality in China, *Sci. Rep.*, 6, 34275, <https://doi.org/10.1038/srep34275>, 2016.

558 Chen, W., Park, J.-K., Dong, B., Lu, R., and Jung, W.-S.: The relationship between El
559 Niño and the western North Pacific summer climate in a coupled GCM: Role of the
560 transition of El Niño decaying phases, *J. Geophys. Res. Atmos.*, 117, D12111,
561 <https://doi.org/10.1029/2011JD017385>, 2012.

562 Cohen, A. J., Brauer, M., Burnett, R., Anderson, H. R., Frostad, J., Estep, K.,
563 Balakrishnan, K., Brunekreef, B., Dandona, L., Dandona, R., Feigin, V., Freedman,
564 G., Hubbell, B., Jobling, A., Kan, H., Knibbs, L., Liu, Y., Martin, R., Morawska, L.,
565 Pope, C. A., Shin, H., Straif, K., Shaddick, G., Thomas, M., van Dingenen, R., van
566 Donkelaar, A., Vos, T., Murray, C. J. L., and Forouzanfar, M. H.: Estimates and
567 25-year trends of the global burden of disease attributable to ambient air pollution:
568 an analysis of data from the Global Burden of Diseases Study 2015, *The Lancet*,
569 389, 1907-1918, [https://doi.org/10.1016/s0140-6736\(17\)30505-6](https://doi.org/10.1016/s0140-6736(17)30505-6), 2017.

570 Feng, J., Zhu, J., and Li, Y.: Influences of El Niño on aerosol concentrations over
571 eastern China, *Atmos. Sci. Lett.*, 17, 422-430, <https://doi.org/10.1002/asl.674>, 2016.

572 Feng, J., Li, J., Zhu, J., Liao, H., and Yang, Y.: Simulated contrasting influences of two
573 La Niña Modoki events on aerosol concentrations over eastern China, *J. Geophys.*
574 *Res. Atmos.*, 122, 2734-2749, <https://doi.org/10.1002/2016JD026175>, 2017.

575 Feng, J., Zhu, J., Li, J., and Liao, H.: Aerosol concentrations variability over China: two
576 distinct leading modes, *Atmos. Chem. Phys.*, 20, 9883-9893,
577 <https://doi.org/10.5194/acp-20-9883-2020>, 2020.

578 Gao, H., and Li, X.: Influences of El Niño Southern Oscillation events on haze
579 frequency in eastern China during boreal winters, *Int. J. Climatol.*, 35, 2682-2688,
580 <https://doi.org/10.1002/joc.4133>, 2015.

581 Golaz, J. C., Caldwell, P. M., Van Roekel, L. P., Petersen, M. R., Tang, Q., Wolfe, J. D.,
582 Abeshu, G., Anantharaj, V., Asay - Davis, X. S., Bader, D. C., Baldwin, S. A., Bisht,
583 G., Bogenschütz, P. A., Branstetter, M., Brunke, M. A., Brus, S. R., Burrows, S. M.,
584 Cameron - Smith, P. J., Donahue, A. S., Deakin, M., Easter, R. C., Evans, K. J.,
585 Feng, Y., Flanner, M., Foucar, J. G., Fyke, J. G., Griffin, B. M., Hannay, C., Harrop,



- 586 B. E., Hoffman, M. J., Hunke, E. C., Jacob, R. L., Jacobsen, D. W., Jeffery, N.,
587 Jones, P. W., Keen, N. D., Klein, S. A., Larson, V. E., Leung, L. R., Li, H. Y., Lin,
588 W., Lipscomb, W. H., Ma, P. L., Mahajan, S., Maltrud, M. E., Mametjanov, A.,
589 McClean, J. L., McCoy, R. B., Neale, R. B., Price, S. F., Qian, Y., Rasch, P. J.,
590 Reeves Eyre, J. E. J., Riley, W. J., Ringler, T. D., Roberts, A. F., Roesler, E. L.,
591 Salinger, A. G., Shaheen, Z., Shi, X., Singh, B., Tang, J., Taylor, M. A., Thornton, P.
592 E., Turner, A. K., Veneziani, M., Wan, H., Wang, H., Wang, S., Williams, D. N.,
593 Wolfram, P. J., Worley, P. H., Xie, S., Yang, Y., Yoon, J. H., Zelinka, M. D., Zender,
594 C. S., Zeng, X., Zhang, C., Zhang, K., Zhang, Y., Zheng, X., Zhou, T., and Zhu, Q.:
595 The DOE E3SM Coupled Model Version 1: Overview and Evaluation at Standard
596 Resolution, *J. Adv. Model. Earth Sys.*, 11, 2089-2129,
597 <https://doi.org/10.1029/2018MS001603>, 2019.
- 598 Grothe, P. R., Cobb, K. M., Liguori, G., Di Lorenzo, E., Capotondi, A., Lu, Y., Cheng,
599 H., Edwards, R. L., Southon, J. R., Santos, G. M., Deocampo, D. M.,
600 Lynch-Stieglitz, J., Chen, T., Sayani, H. R., Thompson, D. M., Conroy, J. L., Moore,
601 A. L., Townsend, K., Hagos, M., O'Connor, G., and Toth, L. T.: Enhanced El
602 Niño-Southern oscillation variability in recent decades, *Geophys. Res. Lett.*, 46,
603 e2019GL083906, <https://doi.org/10.1029/2019GL083906>, 2020.
- 604 Guo, Y., and Tan, Z.: Westward migration of tropical cyclone rapid-intensification over
605 the Northwestern Pacific during short duration El Nino, *Nat. Commun.*, 9, 1507,
606 <https://doi.org/10.1038/s41467-018-03945-y>, 2018.
- 607 Han, X., Zhang, M., Tao, J., Wang, L., Gao, J., Wang, S., and Chai, F.: Modeling aerosol
608 impacts on atmospheric visibility in Beijing with RAMS-CMAQ, *Atmos. Environ.*,
609 72, 177-191, <https://doi.org/10.1016/j.atmosenv.2013.02.030>, 2013.
- 610 Hoesly, R. M., Smith, S. J., Feng, L., Klimont, Z., Janssens-Maenhout, G., Pitkanen, T.,
611 Seibert, J. J., Vu, L., Andres, R. J., Bolt, R. M., Bond, T. C., Dawidowski, L.,
612 Kholod, N., Kurokawa, J.-i., Li, M., Liu, L., Lu, Z., Moura, M. C. P., O'Rourke, P.
613 R., and Zhang, Q.: Historical (1750-2014) anthropogenic emissions of reactive
614 gases and aerosols from the Community Emission Data System (CEDS), *Geosci.
615 Model. Dev.*, 11, 369-408, <https://doi.org/10.5194/gmd-2017-43>, 2018.
- 616 Huang, R.-J., Zhang, Y., Bozzetti, C., Ho, K.-F., Cao, J.-J., Han, Y., Daellenbach, K. R.,
617 Slowik, J. G., Platt, S. M., Canonaco, F., Zotter, P., Wolf, R., Pieber, S. M., Bruns, E.
618 A., Crippa, M., Ciarelli, G., Piazzalunga, A., Schwikowski, M., Abbaszade, G.,
619 Schnelle-Kreis, J., Zimmermann, R., An, Z., Szidat, S., Baltensperger, U., Haddad, I.
620 El, and Prevot, A. S. H.: High secondary aerosol contribution to particulate
621 pollution during haze events in China, *Nature*, 514, 218-222,
622 <https://doi.org/10.1038/nature13774>, 2014.
- 623 Hurrell, J. W., Hack, J. J., Shea, D., Caron, J. M., and Rosinski, J.: A new sea surface
624 temperature and sea ice boundary dataset for the Community Atmosphere Model, *J.
625 Clim.*, 21, 5145-5153, <https://doi.org/10.1175/2008jcli2292.1>, 2008.
- 626 Jeong, J. I., Park, R. J., and Yeh, S. W.: Dissimilar effects of two El Nino types on PM_{2.5}
627 concentrations in East Asia, *Environ. Pollut.*, 242, 1395-1403,



- 628 <https://doi.org/10.1016/j.envpol.2018.08.031>, 2018.
- 629 Jeoung, H., Chung, C. E., Van Noije, T., and Takemura, T.: Relationship between
630 fine-mode AOD and precipitation on seasonal and interannual time scales, *Tellus B*
631 *Chem. Phys. Meteorol.*, 66, <https://doi.org/10.3402/tellusb.v66.23037>, 2014.
- 632 Kao, H-Y., and Yu, J-Y.: Contrasting Eastern-Pacific and Central-Pacific Types of
633 ENSO, *J. Clim.*, 22, 615-632, <https://doi.org/10.1175/2008jcli2309.1>, 2009.
- 634 Li, S., Han, Z., and Chen, H.: A comparison of the effects of interannual Arctic sea ice
635 loss and ENSO on winter haze days: Observational analyses and AGCM
636 simulations, *J. Meteorol. Res.*, 31, 820-833,
637 <https://doi.org/10.1007/s13351-017-7017-2>, 2017.
- 638 Liu, C., Chen, R., Sera, F., Vicedo-Cabrera, A. M., Guo, Y., Tong, S., Coelho, M.S.Z.S.,
639 Saldiva, P. H. N., Lavigne, E., Matus, P., Valdes Ortega, N., Osorio Garcia, S.,
640 Pascal, M., Stafoggia, M., Scortichini, M., Hashizume, M., Honda, Y.,
641 Hurtado-Diaz, M., Cruz, J., Nunes, B., Teixeira, J. P., Kim, H., Tobias, A., Íñiguez,
642 C., Forsberg, B., Åström, C., Ragettli, M. S., Guo, Y.-L., Chen, B.-Y., Bell, M. L.,
643 Wright, C. Y., Scovronick, N., Garland, R. M., Milojevic, A., Kyselý, J., Urban, A.,
644 Orru, H., Indermitte, E., Jaakkola, J. J. K., Rytí, N. R. I., Katsouyanni, K., Analitis,
645 A., Zanobetti, A., Schwartz, J., Chen, J., Wu, T., Cohen, A., Gasparrini, A., and Kan,
646 H.: Ambient Particulate Air Pollution and Daily Mortality in 652 Cities, *N. Engl. J.*
647 *Med.*, 381, 705-715, <https://doi.org/10.1056/NEJMoa1817364>, 2019.
- 648 Liu, Y., Liu, J., and Tao, S.: Interannual variability of summertime aerosol optical depth
649 over East Asia during 2000-2011: a potential influence from El Niño Southern
650 Oscillation, *Environ. Res. Lett.*, 8, 1-9,
651 <https://doi.org/10.1088/1748-9326/8/4/044034>, 2013.
- 652 Rasch, P. J., Xie, S., Ma, P. L., Lin, W., Wang, H., Tang, Q., Burrows, S. M., Caldwell,
653 P., Zhang, K., Easter, R. C., Cameron-Smith, P., Singh, B., Wan, H., Golaz, J. C.,
654 Harrop, B. E., Roesler, E., Bacmeister, J., Larson, V. E., Evans, K. J., Qian, Y.,
655 Taylor, M., Leung, L. R., Zhang, Y., Brent, L., Branstetter, M., Hannay, C.,
656 Mahajan, S., Mamejtanov, A., Neale, R., Richter, J. H., Yoon, J. H., Zender, C. S.,
657 Bader, D., Flanner, M., Foucar, J. G., Jacob, R., Keen, N., Klein, S. A., Liu, X.,
658 Salinger, A. G., Shrivastava, M., and Yang, Y.: An Overview of the Atmospheric
659 Component of the Energy Exascale Earth System Model, *J. Adv. Model Earth Sy.*,
660 11, 2377-2411, <https://doi.org/10.1029/2019MS001629>, 2019.
- 661 Ren, L., Yang, Y., Wang, H., Zhang, R., Wang, P., and Liao, H.: Source attribution of
662 Arctic black carbon and sulfate aerosols and associated Arctic surface warming
663 during 1980-2018, *Atmos. Chem. Phys.*, 20, 9067-9085,
664 <https://doi.org/10.5194/acp-20-9067-2020>, 2020.
- 665 Sakai, K., and Kawamura, R.: Remote response of the East Asian winter monsoon to
666 tropical forcing related to El Niño-Southern Oscillation, *J. Geophys. Res. Atmos.*,
667 114, D06105, <https://doi.org/10.1029/2008JD010824>, 2009.
- 668 Sun, J., Li, H., Zhang, W., Li, T., Zhao, W., Zuo, Z., Guo, S., Wu, D., and Fan, S.:
669 Modulation of the ENSO on Winter Aerosol Pollution in the Eastern Region of



- 670 China, J. Geophys. Res. Atmos., 123, 11,952-11,969,
671 <https://doi.org/10.1029/2018jd028534>, 2018.
- 672 Trenberth, K. E.: El Niño Southern Oscillation (ENSO), Encyclopedia of Ocean
673 Sciences, 420-432, <https://doi.org/10.1016/b978-0-12-409548-9.04082-3>, 2019.
- 674 van Marle, M. J. E., Kloster, S., Magi, B. I., Marlon, J. R., Daniau, A.-L., Field, R. D.,
675 Arneth, A., Forrester, M., Hantson, S., Kehrwald, N. M., Knorr, W., Lasslop, G., Li,
676 F., Mangeon, S., Yue, C., Kaiser, J. W., and van der Werf, G. R.: Historic global
677 biomass burning emissions for CMIP6 (BB4CMIP) based on merging satellite
678 observations with proxies and fire models (1750-2015), Geosci. Model Dev., 10,
679 3329-3357, <https://doi.org/10.5194/gmd-10-3329-2017>, 2017.
- 680 Wang, B., Wu, R., and Fu, X.: Pacific-East Asian Teleconnection: How Does ENSO
681 Affect East Asian Climate?, J. Clim., 13, 1517-1536,
682 [https://doi.org/10.1175/1520-0442\(2000\)013<1517:PEATHD>2.0.CO;2](https://doi.org/10.1175/1520-0442(2000)013<1517:PEATHD>2.0.CO;2), 2000.
- 683 Wang, H., Chen, H., and Liu, J.: Arctic sea ice decline intensified haze pollution in
684 eastern China, Atmos. Ocean Sci. Lett. 8, 1-9,
685 <https://doi.org/10.3878/AOSL20140081>, 2015.
- 686 Wang, H., Easter, R. C., Zhang, R., Ma, P.-L., Singh, B., Zhang, K., Ganguly, D., Rasch,
687 P. J., Burrows, S. M., Ghan, S. J., Lou, S., Qian, Y., Yang, Y., Feng, Y., Flanner, M.,
688 Leung, L. R., Liu, X., Shrivastava, M., Sun, J., Tang, Q., Xie, S., and Yoon, J.-H.,
689 Aerosols in the E3SM Version 1: New developments and their impacts on radiative
690 forcing, J. Adv. Model. Earth Sys., 12, e2019MS001851,
691 <https://doi.org/10.1029/2019MS001851>, 2020.
- 692 Wang, J., Zhu, Z., Qi, L., Zhao, Q., He, J., and Wang, J. X. L.: Two pathways of how
693 remote SST anomalies drive the interannual variability of autumnal haze days in
694 the Beijing-Tianjin-Hebei region, China, Atmos. Chem. Phys., 19, 1521-1535,
695 <https://doi.org/10.5194/acp-19-1521-2019>, 2019.
- 696 Wang, J., Liu, Y., Ding, Y., Wu, P., Zhu, Z., Xu, Y., Li, Q., Zhang, Y., He, J., Wang, J. X.
697 L., and Qi, L.: Impacts of climate anomalies on the interannual and interdecadal
698 variability of autumn and winter haze in North China: A review, Int. J. Climatol., 40,
699 4309-4325, <https://doi.org/10.1002/joc.6471>, 2020a.
- 700 Wang, J., Liu, Y., and Ding, Y.: On the connection between interannual variations of
701 winter haze frequency over Beijing and different ENSO flavors, Sci. Total Environ.,
702 740, 140109, <https://doi.org/10.1016/j.scitotenv.2020.140109>, 2020b.
- 703 Wu, X., Okumura, Y. M., and Dinezio, P. N.: What Controls the Duration of El Niño
704 and La Niña Events?, J. Clim., 32, 5941-5965,
705 <https://doi.org/10.1175/jcli-d-18-0681.1>, 2019.
- 706 Yang, Y., Liao, H., and Li, J.: Impacts of the East Asian summer monsoon on
707 interannual variations of summertime surface-layer ozone concentrations over
708 China, Atmos. Chem. and Phys., 14, 6867-6879,
709 <https://doi.org/10.5194/acp-14-6867-2014>, 2014.
- 710 Yang, Y., Liao, H., and Lou, S.: Increase in winter haze over eastern China in recent
711 decades: Roles of variations in meteorological parameters and anthropogenic



- 712 emissions, *J. Geophys. Res. Atmos.*, 121, 13050-13065,
713 <https://doi.org/10.1002/2016JD025136>, 2016a.
- 714 Yang, Y., Russell, L. M., Xu, L., Lou, S., Lamjiri, M. A., Somerville, R. C. J., Miller, A.
715 J., Cayan, D. R., DeFlorio, M. J., Ghan, S. J., Liu, Y., Singh, B., Wang, H., Yoon,
716 J.-H., and Rasch, P. J.: Impacts of ENSO events on cloud radiative effects in
717 preindustrial conditions: Changes in cloud fraction and their dependence on
718 interactive aerosol emissions and concentrations, *J. Geophys. Res. Atmos.*, 121,
719 6321-6335, <https://doi.org/10.1002/2015jd024503>, 2016b.
- 720 Yang, Y., Russell, L. M., Lou, S., Liu, Y., Singh, B., and Ghan, S. J.: Rain-aerosol
721 relationships influenced by wind speed, *Geophys. Res. Lett.*, 43, 2267-2274,
722 <https://doi.org/10.1002/2016GL067770>, 2016c.
- 723 Yang, Y., Wang, H., Smith, S. J., Easter, R., Ma, P.-L., Qian, Y., Yu, H., Li, C., and
724 Rasch, P. J.: Global source attribution of sulfate concentration and direct and
725 indirect radiative forcing, *Atmos. Chem. Phys.*, 17, 8903-8922,
726 <https://doi.org/10.5194/acp-17-8903-2017>, 2017a.
- 727 Yang, Y., Wang, H., Smith, S. J., Ma, P.-L., and Rasch, P. J.: Source attribution of black
728 carbon and its direct radiative forcing in China, *Atmos. Chem. Phys.*, 17,
729 4319-4336, <https://doi.org/10.5194/acp-17-4319-2017>, 2017b.
- 730 Yang, Y., Wang, H., Smith, S. J., Zhang, R., Lou, S., Qian, Y., Ma, P.-L., and Rasch, P. J.:
731 Recent intensification of winter haze in China linked to foreign emissions and
732 meteorology, *Sci. Rep.*, 8, 2107, <https://doi.org/10.1038/s41598-018-20437-7>,
733 2018.
- 734 Yang, Y., Lou, S., Wang, H., Wang, P., and Liao, H.: Trends and source apportionment
735 of aerosols in Europe during 1980-2018, *Atmos. Chem. Phys.*, 20, 2579-2590,
736 <https://doi.org/10.5194/acp-20-2579-2020>, 2020.
- 737 Yu, X., Wang, Z., Zhang, H., and Zhao, S.: Impacts of different types and intensities of
738 El Nino events on winter aerosols over China, *Sci. Total Environ.*, 655, 766-780,
739 <https://doi.org/10.1016/j.scitotenv.2018.11.090>, 2019.
- 740 Zhang, G., Gao, Y., Cai, W., Leung, L. R., Wang, S., Zhao, B., Wang, M., Shan, H., Yao,
741 X., and Gao, H.: Seesaw haze pollution in North China modulated by the
742 sub-seasonal variability of atmospheric circulation, *Atmos. Chem. Phys.*, 19,
743 565-576, <https://doi.org/10.5194/acp-19-565-2019>, 2019.
- 744 Zhang, Z., Gong, D., Mao, R., Kim, S.-J., Xu, J., Zhao, X., and Ma, Z.: Cause and
745 predictability for the severe haze pollution in downtown Beijing in
746 November-December 2015, *Sci. Total Environ.*, 592, 627-638,
747 <https://doi.org/10.1016/j.scitotenv.2017.03.009>, 2017.
- 748 Zhao, S., Li, J. P., and Sun, C.: Decadal variability in the occurrence of wintertime haze
749 in central eastern China tied to the Pacific decadal oscillation, *Sci. Rep.*, 6, 27424,
750 <https://doi.org/10.1038/srep27424>, 2016.
- 751 Zhao, B., Wu, W., Wang, S., Xing, J., Chang, X., Liou, K.-N., Jiang, J. H., Gu, Y., Jang,
752 C., Fu, J. S., Zhu, Y., Wang, J., Lin, Y., and Hao, J.: A modeling study of the
753 nonlinear response of fine particles to air pollutant emissions in the



754 Beijing-Tianjin-Hebei region, *Atmos. Chem. Phys.*, 17, 12031-12050,
755 <https://doi.org/10.5194/acp-17-12031-2017>, 2017.
756 Zhao, S., Zhang, H., and Xie, B.: The effects of El Niño-Southern Oscillation on the
757 winter haze pollution of China, *Atmos. Chem. and Phys.*, 18, 1863-1877,
758 <https://doi.org/10.5194/acp-18-1863-2018>, 2018.
759 Zhu, J., Liao, H., and Li, J.: Increases in aerosol concentrations over eastern China due
760 to the decadal-scale weakening of the East Asian summer monsoon, *Geophys. Res.*
761 *Lett.*, 39, L09809, <https://doi.org/10.1029/2012GL051428>, 2012.
762 Zou, Y., Wang, Y., Xie, Z., Wang, H., and Rasch, P. J.: Atmospheric teleconnection
763 processes linking winter air stagnation and haze extremes in China with regional
764 Arctic sea ice decline, *Atmos. Chem. Phys.*, 20, 4999-5017, 2020.
765
766



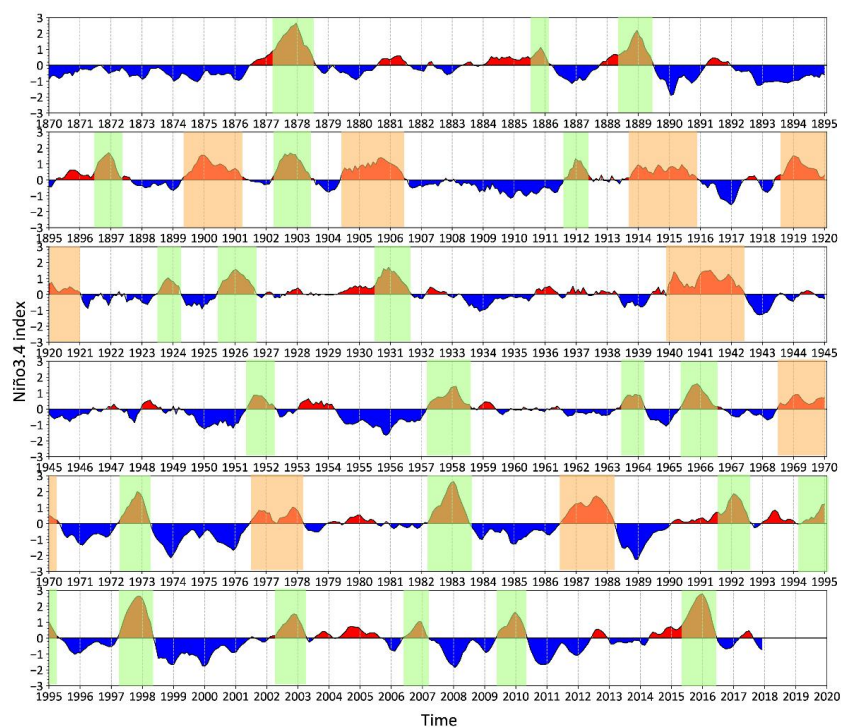
767 **Table 1.** The seasonal mean aerosol concentrations (unit: $\mu\text{g m}^{-3}$) and number of haze days (unit:
 768 day) in December-January-February (DJF) over various regions of China, including NCP, SCB,
 769 YRD, PRD, NEP, YGP, and FWP from CLIM, SD and LD experiments. Haze days are defined as
 770 days with daily average near-surface $\text{PM}_{2.5}$ concentrations above the 90th percentile in each region.
 771 The values in brackets represent the anomalies in SD and LD relative to CLIM.
 772

		NCP	SCB	YRD	PRD	NEP	YGP	FWP
Mean Conc.	CLIM	24.87	32.33	27.98	17.26	9.42	20.19	25.11
	SD	23.73 (-1.14)	31.16 (-1.17)	28.21 (+0.23)	18.20 (+0.94)	9.95 (+0.53)	19.55 (-0.64)	23.17 (-1.94)
	LD	24.76 (-0.11)	32.09 (-0.24)	27.84 (-0.14)	18.09 (+0.83)	9.71 (+0.29)	20.07 (-0.12)	24.64 (-0.47)
Haze Days	CLIM	9.00	9.00	9.00	9.00	9.00	9.00	9.00
	SD	7.20 (-1.87)	6.87 (-2.13)	9.87 (+0.87)	10.27 (+1.27)	10.87 (+1.80)	7.60 (-1.40)	6.13 (-2.87)
	LD	7.93 (-1.14)	8.27 (-0.73)	9.53 (+0.53)	11.07 (+2.07)	10.00 (+0.93)	9.40 (+0.40)	7.47 (-1.53)

773
 774
 775
 776



777

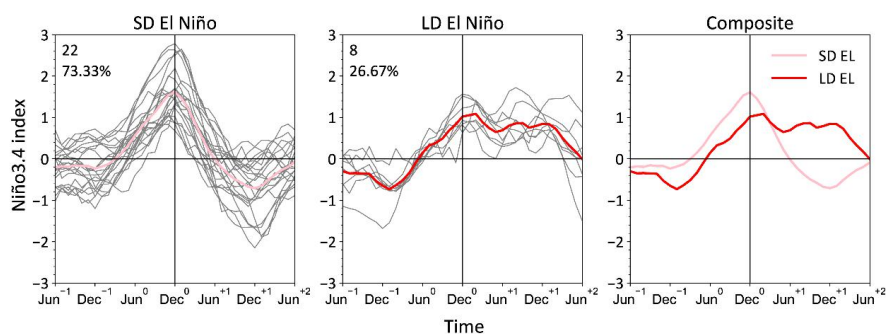


778

779 **Figure 1.** Time series of the Niño3.4 index (°C) based on the merged Hadley-NOAA/OI SST
780 dataset for 1870-2017. The time series were detrended and smoothed with a 3-month running
781 average filter. Highlighted slots illustrate the SD (green) and LD (orange) El Niño events.

782

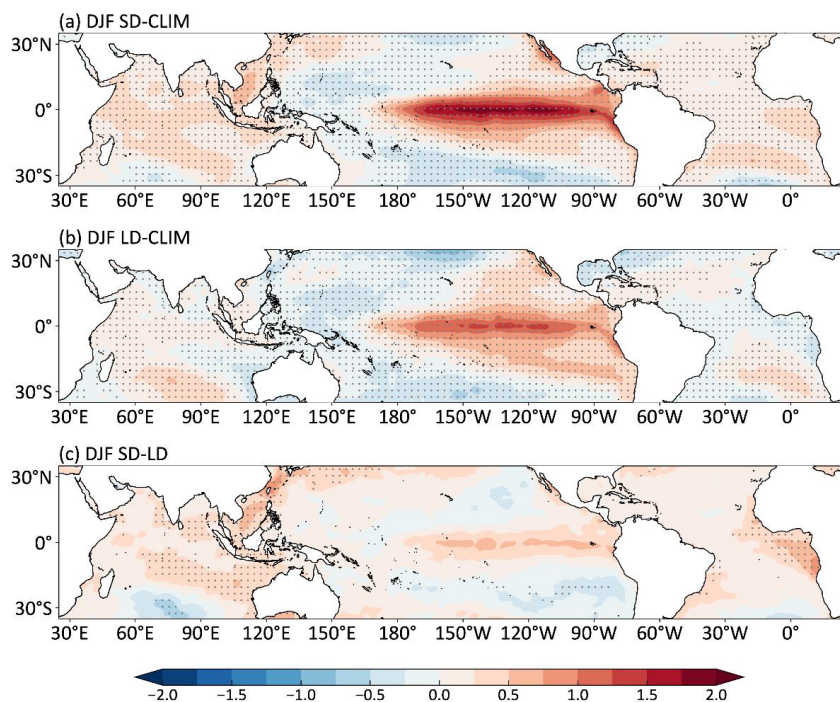
783



784

785

786 **Figure 2.** Time series of the Niño3.4 index (°C) overlaid from Jun⁻¹ to Jun⁺² for (left) SD and
787 (middle) LD El Niño events during 1870-2017. The individual and composite events are shown by
788 thin gray and bold red curves, respectively. The total number and percentage of events are shown
789 at the upper left corner of each panel. A comparison of the composite time series of Niño3.4 index
790 for SD and LD events is shown in the right panel.



791

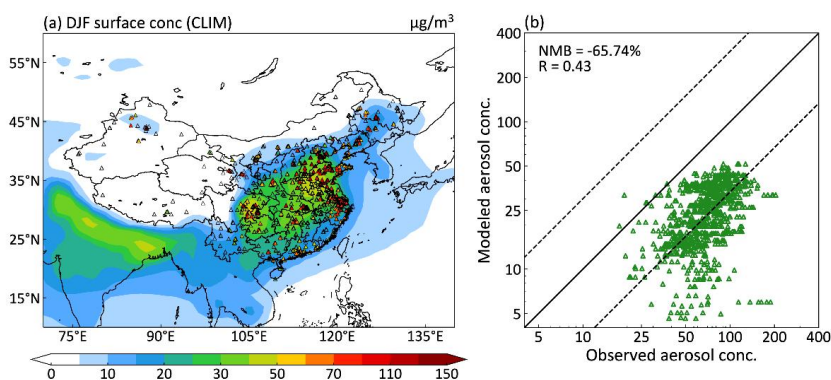
792

793 **Figure 3.** Composite differences in DJF mean SST (°C) between SD (a) / LD (b) El Niño events
794 and climatological mean over 1870-2017 and between SD and LD (c) El Niño events. Differences
795 that are statistically significant at 95% from a two-tailed T-test are stippled.

796



797



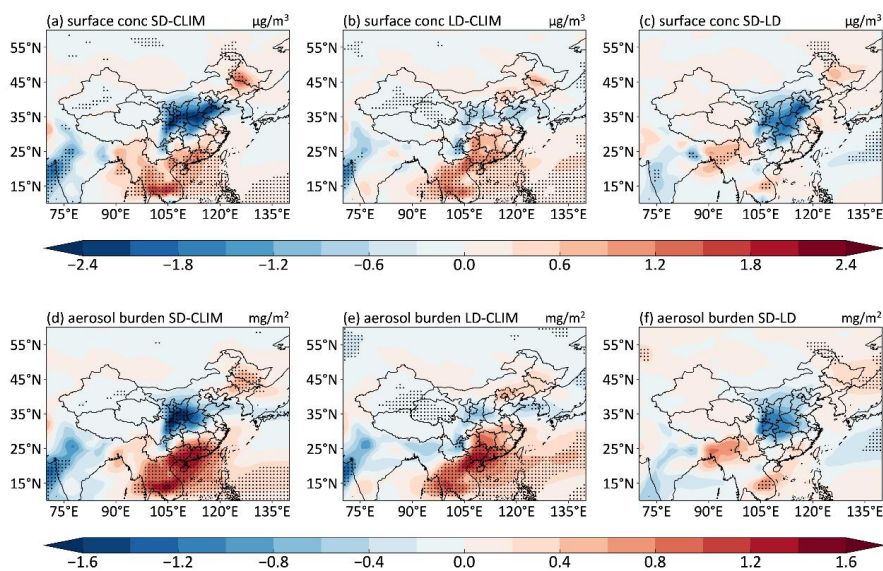
798

799

800 **Figure 4.** Spatial distributions (a) and scatter plots (b) of observed and simulated DJF mean
801 near-surface PM_{2.5} concentrations ($\mu\text{g m}^{-3}$) from the CLIM experiment. Solid line represents 1:1
802 ratio and dashed lines mark 1:3 and 3:1 ratios. The observed concentrations are derived from the
803 CNEMC in December 2014–February 2015. The normalized mean deviation (NMB) and the
804 correlation coefficient (R) between observations and simulation are shown in the upper left corner
805 of the right panel. $\text{NMB} = 100\% \times \sum (M_i - O_i) / \sum O_i$, where M_i and O_i are the simulated and
806 observed values at the site i , respectively.

807

808

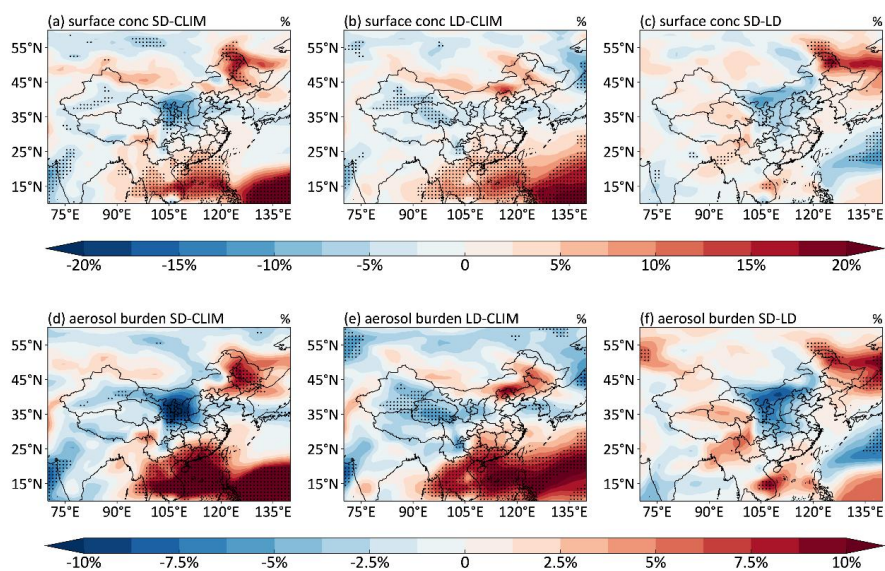


809

810

811 **Figure 5.** Composite differences in DJF mean near-surface $\text{PM}_{2.5}$ concentrations ($\mu\text{g m}^{-3}$) and
812 aerosol column burdens (mg m^{-2}) between SD and CLIM (a, d), LD and CLIM (b, e), and SD and
813 LD (c, f). The stippled areas indicate statistical significance with 90% confidence from a
814 two-tailed T-test.

815



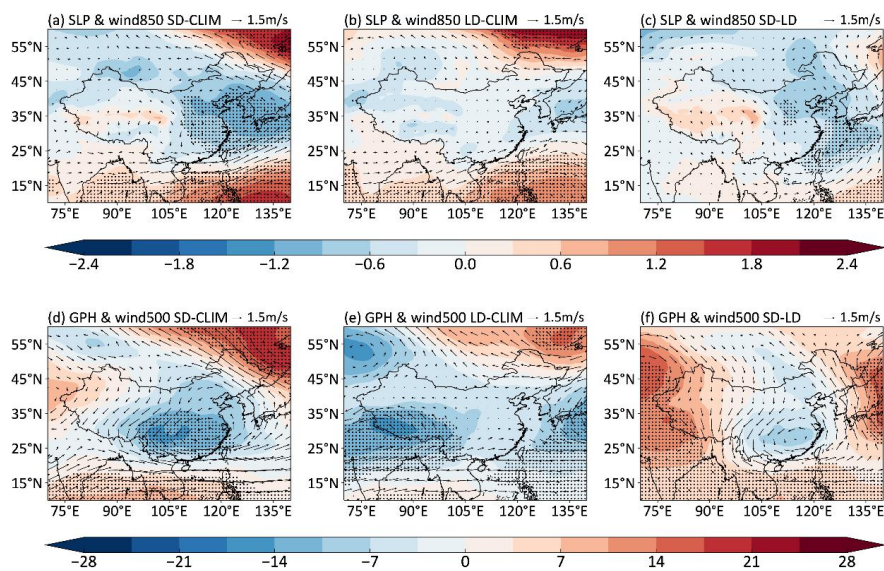
816

817

818 **Figure 6.** Composite differences (%) in DJF mean near-surface $PM_{2.5}$ concentrations and aerosol
819 column burdens between SD and CLIM (a, d), LD and CLIM (b, e), and SD and LD (c, f), relative
820 to CLIM. The stippled areas indicate statistical significance with 90% confidence from a
821 two-tailed T-test.



822



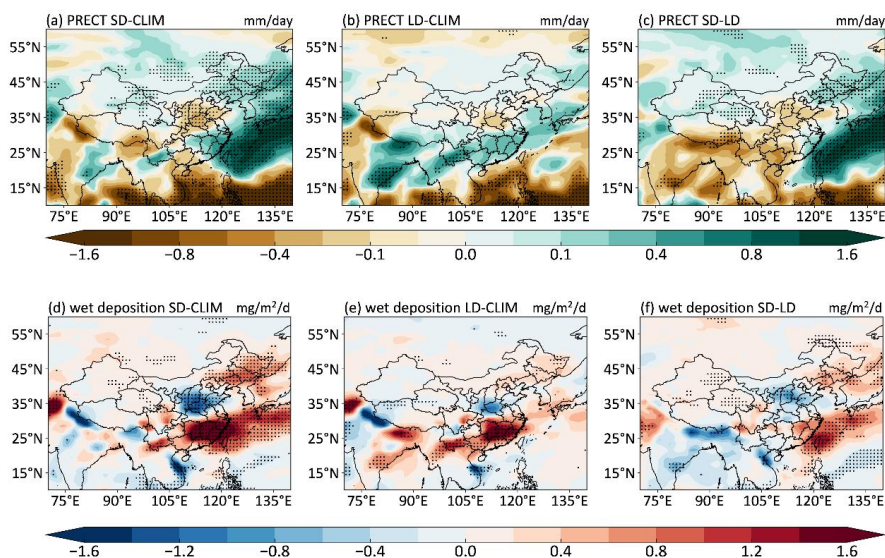
823

824

825 **Figure 7.** Composite differences in DJF mean sea level pressure (SLP, shaded; units: hPa) and
826 wind at 850 hPa (WIND850, vector; units: m s^{-1}) (top panels) and geopotential height at 500 hPa
827 (GPH500, shaded; units: m) and wind at 500 hPa (WIND500, vector; units: m s^{-1}) (bottom panels)
828 between SD and CLIM (a, d), LD and CLIM (b, e), and SD and LD (c, f). The stippled areas
829 indicate statistical significance with 90% confidence from a two-tailed T-test.



830



831

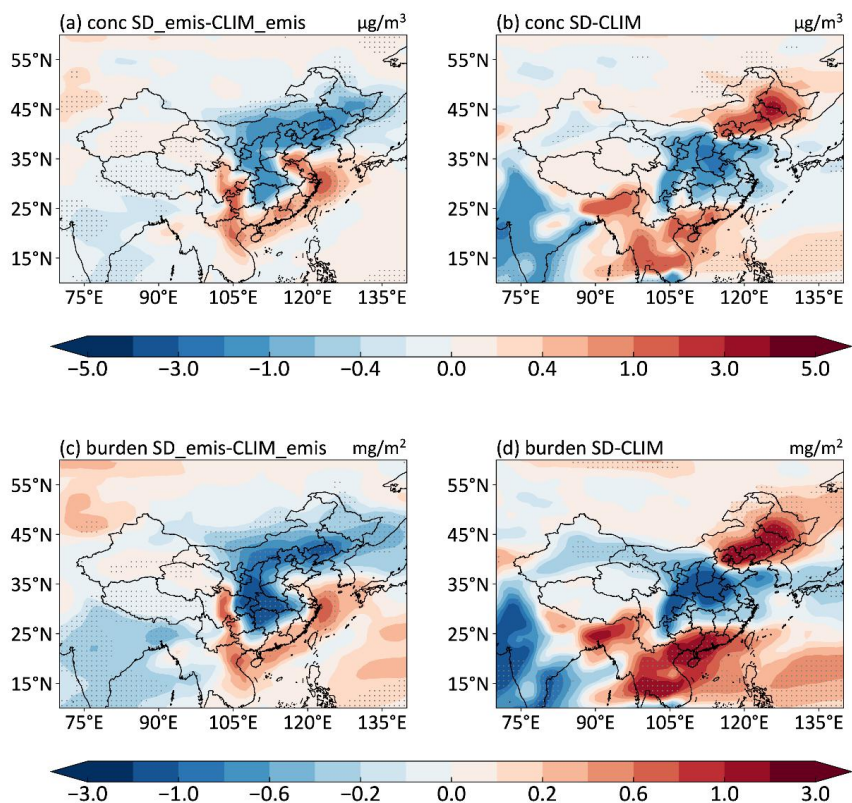
832

833 **Figure 8.** Composite differences in DJF mean precipitation rate (top panels; units: mm day^{-1}) and
834 wet deposition of $\text{PM}_{2.5}$ (bottom panels; units: $\text{mg m}^{-2} \text{d}^{-1}$) between SD and CLIM (a, d), LD and
835 CLIM (b, e), and SD and LD (c, f). The stippled areas indicate statistical significance with 90%
836 confidence from a two-tailed T-test.

837



838



839

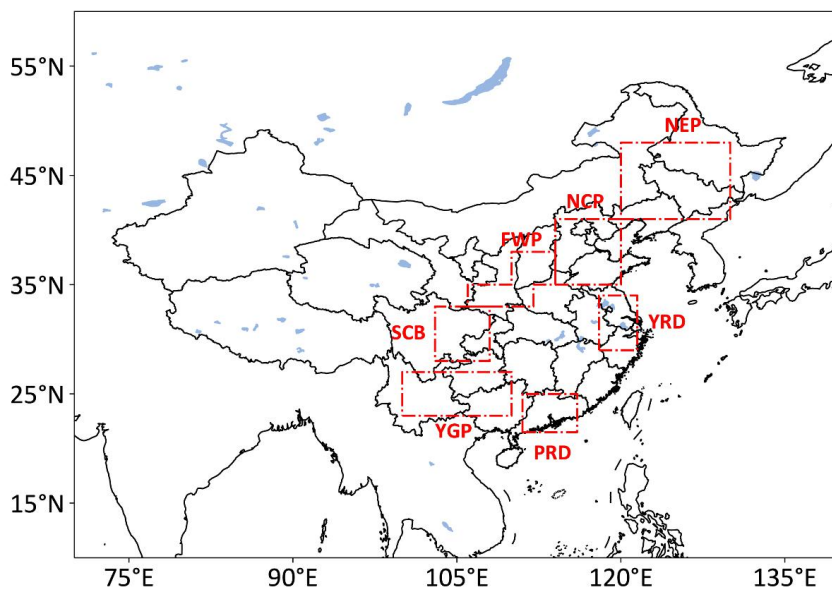
840

841 **Figure 9.** Composite differences in DJF mean near-surface $\text{PM}_{2.5}$ concentration ($\mu\text{g m}^{-3}$) and

842 aerosol column burden (mg m^{-2}) between SD_emis and CLIM_emis (a, c) SD and CLIM (b, d).

843 The stippled areas indicate statistical significance with 90% confidence from a two-tailed T-test.

844



845

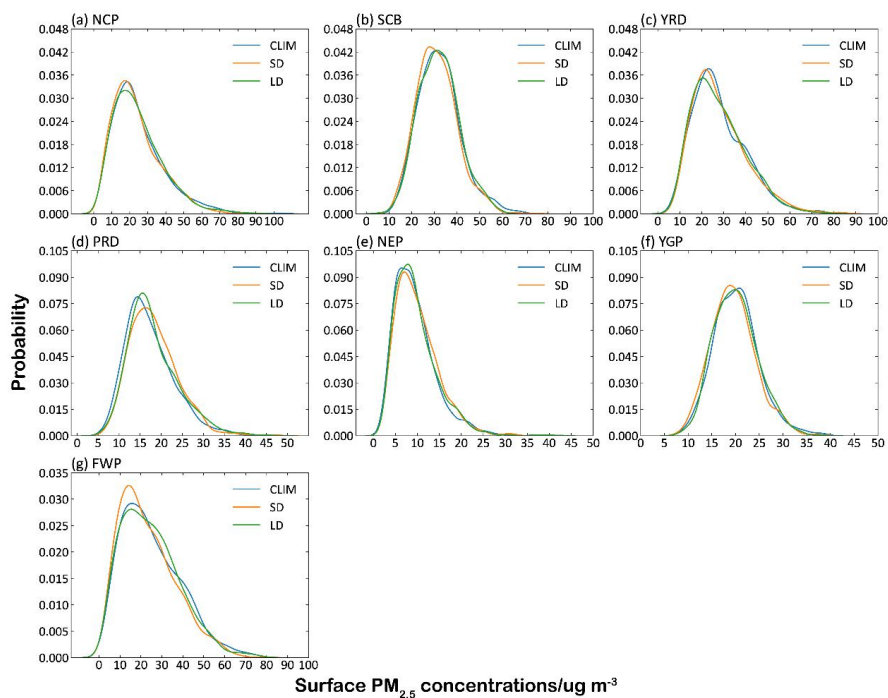
846

847 **Figure 10.** Subregions of China defined in this study, including the North China Plain (NCP,
848 35–41°N, 114–120°E), the Sichuan Basin (SCB, 28–33°N, 103–108°E), the Yangtze River Delta
849 (YRD, 29–34°N, 118–121.5°E), the Pearl River Delta (PRD, 21.5–25°N, 111–116°E), the
850 Northeast Plain (NEP, 41–48°N, 120–130°E), the Yunnan-Guizhou Plateau (YGP, 23–27°N,
851 100–110°E), and the Fenwei Plain (FWP, 33–35°N, 106–112°E and 35–38°N, 110–114°E).

852



853



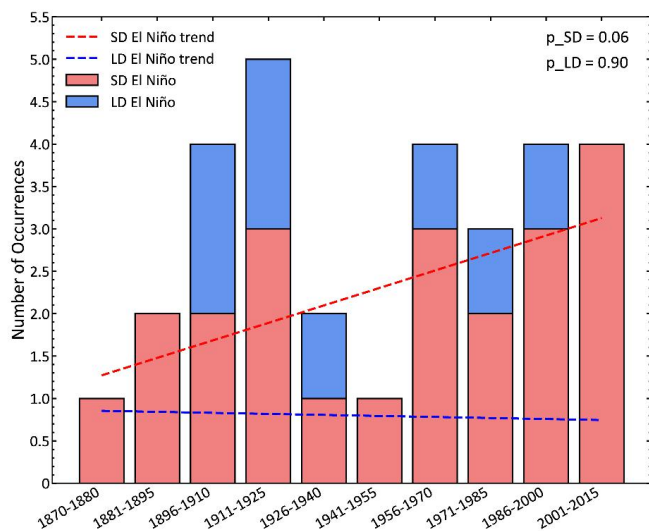
854

855

856 **Figure 11.** Probability density distributions of daily near-surface PM_{2.5} concentrations (µg m⁻³) in
857 DJF over various subregions of China.

858

859



860

861

862 **Figure 12.** Stacked histograms of the number of SD and LD El Niño events per 15 years (except
863 1870-1880 for 10 years) during 1870-2015. The red and blue dashed lines indicate linear trends in
864 the number of SD and LD El Niño events, respectively. Their p-values are shown in the upper
865 right corner of the figure, which indicate the increasing trend of SD at a two-tailed T-test
866 confidence level of 94% for 1870-2015 (87% for 1880-2015 and 92% for 1940-2015) statistical
867 significance.

868

869